Experimental determination of acoustic properties using a two-microphone random-excitation technique*

A. F. Seybert

Mechanical Engineering Department, University of Kentucky, Lexington, Kentucky 40506

D. F. Ross

Arvin Industries, Incorporated, Lafayette, Indiana 47906
(Received 17 December 1976)

An experimental technique is presented for the determination of normal acoustic properties in a tube, including the effect of mean flow. An acoustic source is driven by Gaussian white noise to produce a randomly fluctuating sound field in a tube terminated by the system under investigation. Two stationary, wall-mounted microphones measure the sound pressure at arbitrary but known positions in the tube. Theory is developed, including the effect of mean flow, showing that the incident- and reflected-wave spectra, and the phase angle between the incident and reflected waves, can be determined from measurement of the auto- and cross-spectra of the two microphone signals. Expressions for the normal specific acoustic impedance and the reflection coefficient of the tube termination are developed for a random sound field in the tube. Three no-flow test cases are evaluated using the two-microphone random-excitation technique: a closed tube of specified length, an open, unbaffled tube of specified length, and a prototype automotive muffler. Comparison is made between results using the present method and approximate theory and results from the traditional standing-wave method. In all cases agreement between the two-microphone random-excitation method and comparison data is excellent. The two-microphone random-excitation technique can be used to evaluate acoustic properties very rapidly since no traversing is necessary and since random excitation is used (in each of three test cases only 7 sec of continuous data was needed). In addition, the bandwidth may be made arbitrarily small, within limits, so that the computed properties will have a high degree of frequency resolution.

PACS numbers: 43.85.Bh, 43.50.Gf, 43.20.Mv

LIST OF SYMBOLS

$\tilde{a}(t)$	amplitude of incident wave
$\tilde{b}(t)$	amplitude of reflected wave
$\tilde{A}$	Fourier transform of incident wave amplitude
$\tilde{B}$	Fourier transform of reflected wave amplitude
c	speed of sound in still air
c_0	speed of wave propagation in presence of flow
f	frequency
k	wave number without flow
k_i	wave number in direction of flow
k_r	wave number in opposite direction of flow
L	tube length
M	mean flow Mach number
$\tilde{p}_i$	incident wave pressure
$\tilde{p}_r$	reflected wave pressure
$\tilde{p}$	total acoustic pressure
$\tilde{P}_j$	Fourier transform of total acoustic pressure at $x=x_j$
R	complex pressure reflection coefficient
$\hat{R}_n$	estimate of the resistive impedance
$\hat{S}_{uu}$	estimate of the auto-spectral density of $\tilde{u}$ at $x=0$
$\hat{S}_{pp}$	estimate of the auto-spectral density of $\tilde{p}$ at $x=0$
$\hat{S}_{pu}$	estimate of the cross-spectral density between $\tilde{p}$ and $\tilde{u}$ at $x=0$
$\hat{S}_{AA}$	estimate of the auto-spectral density of $\tilde{a}(t)$
$\hat{S}_{BB}$	estimate of the auto-spectral density of $\tilde{b}(t)$
$\hat{S}_{AB}$	estimate of the cross-spectral density between $\tilde{a}(t)$ and $\tilde{b}(t)$
$\hat{C}_{AB}$, $\hat{Q}_{AB}$	real and imaginary parts of $\hat{S}_{AB}$, respectively.
$\hat{S}_{11}$	estimate of the auto-spectral density of $\tilde{p}_1$
$\hat{S}_{22}$	estimate of the auto-spectral density of $\tilde{p}_2$
$\hat{S}_{12}$	estimate of the cross-spectral density between $\tilde{p}_1$ and $\tilde{p}_2$
$\hat{C}_{12}$, $\hat{Q}_{12}$	real and imaginary parts of $\hat{S}_{12}$, respectively
t	time coordinate
T	total length of data record
TL	transmission loss
$\tilde{u}_i$	incident wave particle velocity
$\tilde{u}_r$	reflected wave particle velocity
$\tilde{u}$	total acoustic particle velocity
$\tilde{U}_j$	Fourier transform of total acoustic particle velocity at $x=x_j$
v	mean flow velocity
x	spatial coordinate
x_1	position of first microphone
x_2	position of second microphone
$\hat{Z}_n$	estimate of the impedance
$\hat{\alpha}_n$	estimate of the power reflection coefficient
$\hat{\theta}$	estimate of the phase angle at $x=0$
λ	wavelength
ρ	air density
$\hat{\chi}$	estimate of the reactive impedance
ω	angular frequency

INTRODUCTION

In many practical problems acoustic properties such as normal acoustic resistance and reactance, normal reflection, absorption and transmission coefficients, and transmission loss cannot be determined analytically. Owing to complex geometry, the presence of mean flow, or other reasons, experimental techniques must be used.

Several techniques have been used to determine the normal incidence properties of acoustic systems. The most popular is the standing-wave-ratio (SWR) method where a traversing microphone is used to determine the location and magnitude of successive maxima and minima of the standing-wave pattern in a tube terminated by the unknown system. From this information the normal acoustic impedance and reflection coefficient can be deduced. The technique can be time consuming since the traversing mechanism is usually operated manually and discrete frequency excitation is used. It is recommended[1] that the tube be at least one wavelength long, which is somewhat unwieldy at low frequencies. It is also suggested that the results be corrected for dissipation[2] if higher accuracy is desired. Errors can also occur if the location of the first minimum is not known to a high degree of accuracy. In addition, it may not be possible to use a traversing microphone if the system under study has a small diameter.

Gatley[3] considered the use of a pulse or transient method with a wall-mounted microphone but concluded the technique had the disadvantage of requiring a long tube length, which is inconvenient and results in significant dissipation. The method discussed by Gatley is also somewhat laborious since it is a discrete frequency approach. He used a gated sine wave to excite the system, where the duration of the sine-wave excitation was long enough to reach steady state, but short enough to separate in time the incident and reflected waves.

Recently, Schmidt and Johnston[4] used a discrete-frequency technique, to evaluate orifices, employing two wall-mounted microphones at different upstream positions along a tube (note: this should not be confused with the so-called "two-microphone method" used to measure the impedance of porous resonant expansion chambers[5]). By measuring the pressure amplitudes at the two points in the tube, as well as the phase shift between the points, they deduced the reflection coefficient of the sample. Their method did not include the determination of reactive and resistive impedance, but a third microphone located downstream of the orifice was used to measure the transmitted wave amplitude from which they computed transmission coefficients.

Singh and Katra[6] have developed an acoustic impulse method to determine the properties of small filters used on refrigeration compressors. They used a wall-mounted microphone located midway along a tube connecting an acoustic driver to the system being tested. The excitation was provided by a rectangular pulse of very short duration supplied to the acoustic driver. A short duration pulse in conjunction with a long tube allowed separation of the incident and reflected pulses in the time domain. They repeated the experiment about 100 times to obtain ensemble-averaged time domain signals for the incident and reflected pulses. Ensemble averaging in the time domain removed random pressure oscillations (such as from flow) from the incident and reflected pulses. They also used a second microphone downstream of the system to measure the transmitted pulse for use in computing transmission loss.

Since they performed ensemble averaging in the time domain, the pulse exciting the system had to be very repeatable from sample to sample and accurate synchronization between the samples was crucial. They found it necessary to construct the pulses digitally to satisfy these demands, where a digital-to-analog converter was used to generate the corresponding voltage signal supplied to the acoustic driver. An additional constraint involved the selection of the tube length and pulse duration. The tube must be long enough to allow time domain separation of the incident and reflected pulses without introducing excessive dissipative losses, a problem also encountered by Gatley.

One of the problems in using impulse testing with acoustic systems is the difficulty in producing an acoustic pulse which has sufficient energy at high frequencies to provide an acceptable signal-to-noise ratio between the pulse and flow and/or background noise. Even acoustic drivers with a wide frequency range are usually underdamped, resulting in long transients even when the excitation approaches a true impulse. A better source of pulse excitation for acoustic systems is the electric spark; however, it may not be sufficiently repeatable for the impulse method of Singh and Katra.

The remainder of this paper will discuss a method using two upstream microphones, similar to Ref. 4, where here the excitation is band-limited white noise. Theory is developed relating to the auto- and cross-spectral densities of the incident and reflected waves to the auto- and cross-spectral densities of the two measurement points. The acoustic impedance and absorption coefficient are expressed in terms of the auto- and cross-spectral densities of the incident and reflected waves, analogous to the case of discrete harmonic excitation. The effect of mean flow is included in the theory. A third microphone (downstream) is used to compute transmission loss, usually the most important parameter in evaluating acoustic filters.

I. DESCRIPTION OF TECHNIQUE

Figure 1 is a diagram showing a rigid tube excited by a randomly vibrating piston, or other acoustic source, and terminated by an acoustic system with unknown impedance $Z_n(f)$ and unknown reflection coefficient $\alpha_n(f)$. Mean flow is included where v is the velocity of the fluid. Also, the piston vibration is assumed to be stationary with time. The origin of the coordinate system is at the termination of the tube and x_1 and x_2 are the distances to two pressure measurement points. The incident and reflected pressure waves are denoted by $\tilde{p}_i$ and $\tilde{p}_r$, respectively.

In a narrow bandwidth B_e, centered at frequency f,

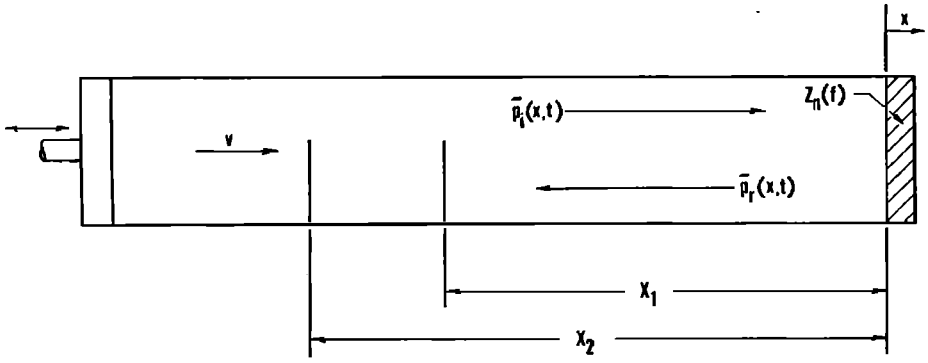

FIG. 1. Tube with unknown termination impedance $Z_n(f)$ excited by randomly vibrating piston.

random motion can be regarded as harmonic motion of frequency f with a randomly varying amplitude. For plane-wave propagation the incident and reflected waves are given by

$$\tilde{p}_i(x,t)=\tilde{a}(t)e^{i(\omega t-kx)},$$

$$\tilde{p}_r(x,t)=\tilde{b}(t)e^{i(\omega t+kx)},$$

where

$\omega=2\pi f$,

$k=\omega/c_0$ = acoustic wave number,

c_0 = speed of propagation,

and $\tilde{a}(t)$ and $\tilde{b}(t)$ are stationary random variables. The random amplitudes $\tilde{a}(t)$ and $\tilde{b}(t)$ are not functions of distance x since the system is nondispersive; therefore, the wave shape does not change during propagation.

The influence of flow can be included by noting that

$c_0=c+v$ for wave motion with flow,

$c_0=c-v$ for wave motion against flow,

where c is the speed of propagation with zero flow. For flow in the $+x$ direction, the incident and reflected wave numbers are given by

$$k_i=\frac{\omega}{c+v}=\frac{k}{1+M},$$

$$k_r=\frac{\omega}{c-v}=\frac{k}{1-M},$$

where $M=v/c$ is the Mach number. Consequently, the incident and reflected waves are

$$\tilde{p}_i(x,t)=\tilde{a}(t)e^{i(\omega t-k_i x)}, \tag{1a}$$

$$\tilde{p}_r(x,t)=\tilde{b}(t)e^{i(\omega t+k_r x)}. \tag{1b}$$

At $x=0$ the total pressure and particle velocity are

$$\tilde{p}(0,t)=[\tilde{a}(t)+\tilde{b}(t)]e^{i\omega t}, \tag{2}$$

$$\tilde{u}(0,t)=\tilde{u}_i(0,t)+\tilde{u}_r(0,t),$$

where $\tilde{u}_i(x,t)$ and $\tilde{u}_r(x,t)$ are the particle velocities of the incident and reflected waves, respectively. Since

$$\tilde{u}_i(x,t)=\tilde{p}_i(x,t)/\rho c,\quad \tilde{u}_r(x,t)=-\tilde{p}_r(x,t)/\rho c,$$

then

$$\tilde{u}(0,t)=[\tilde{a}(t)-\tilde{b}(t)]\frac{e^{i\omega t}}{\rho c}. \tag{3}$$

The impedance $Z_n(f)$ can be regarded as a linear system that relates the total pressure and velocity at $x=0$, represented by the block diagram in Fig. 2. From linear theory[7] it can be shown that $Z_n(f)$ is estimated by

$$\hat{Z}_n(f)=\hat{S}_{pu}(f)/\hat{S}_{uu}(f), \tag{4}$$

where $\hat{S}_{pu}(f)$ is an estimate of the cross-spectral density between the pressure and particle velocity at $x=0$ and $\hat{S}_{uu}(f)$ is an estimate of the auto-spectral density of the particle velocity at $x=0$. These spectra are estimated by

$$\hat{S}_{pu}(f)=(1/T)\{\tilde{P}_0(f,T)\tilde{U}_0^*(f,T)\}, \tag{5a}$$

$$\hat{S}_{uu}(f)=(1/T)\{\tilde{U}_0(f,T)\tilde{U}_0^*(f,T)\}. \tag{5b}$$

The auto-spectra of the pressure at $x=0$, $\hat{S}_{pp}(f)$, is estimated by

$$\hat{S}_{pp}(f)=(1/T)\{\tilde{P}_0(f,T)\tilde{P}_0^*(f,T)\}. \tag{5c}$$

In Eqs. (5a), (5b), and (5c), $\tilde{P}_0(f,T)$ and $\tilde{U}_0(f,T)$ are the finite Fourier transforms of the pressure and particle velocity time series at $x=0$, respectively,

$$\tilde{P}_0(f,T)=\frac{1}{T}\int_0^T\tilde{p}(0,t)e^{-i\omega t}dt, \tag{6a}$$

$$\tilde{U}_0(f,T)=\frac{1}{T}\int_0^T\tilde{u}(0,t)e^{-i\omega t}dt, \tag{6b}$$

where T is the record length of the time series and the asterisk denotes complex conjugate.

Using Eqs. (2), (3), (6a), and (6b):

$$\tilde{P}_0(f,T)=\tilde{A}(f,T)+\tilde{B}(f,T), \tag{7a}$$

$$\tilde{U}_0(f,T)=[\tilde{A}(f,T)-\tilde{B}(f,T)](1/\rho c), \tag{7b}$$

where $\tilde{A}(f,T)$ and $\tilde{B}(f,T)$ are the finite Fourier transforms of $\tilde{a}(t)$ and $\tilde{b}(t)$, respectively.

Substituting Eqs. (7a) and (7b) into the spectral densities [Eqs. (5a), (5b), and (5c)] yields

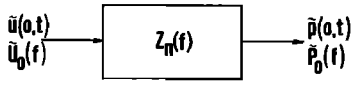

FIG. 2. Block diagram showing relationship between acoustic impedance, pressure, and particle velocity.

$$\hat{S}_{pu}(f) = (1/\rho c)[\hat{S}_{AA}(f) - \hat{S}_{BB}(f) - i2\hat{Q}_{AB}(f)], \quad (8a)$$

$$\hat{S}_{uu}(f) = (1/\rho c)^2[\hat{S}_{AA}(f) - \hat{S}_{BB}(f) - 2\hat{C}_{AB}(f)], \quad (8b)$$

$$\hat{S}_{pp}(f) = \hat{S}_{AA}(f) + \hat{S}_{BB}(f) + 2\hat{C}_{AB}(f). \quad (8c)$$

$\hat{S}_{AA}(f)$ and $\hat{S}_{BB}(f)$ are the auto-spectral densities of the incident and reflected waves, respectively; $\hat{C}_{AB}(f)$ and $\hat{Q}_{AB}(f)$ are the real and imaginary components of the cross-spectral density $\hat{S}_{AB}(f)$ between the incident and reflected waves:

$$\hat{S}_{AB}(f) = \hat{C}_{AB}(f) + i\hat{Q}_{AB}(f).$$

Consequently, the acoustic impedance [Eq. (4)] is expressed by

$$\frac{\hat{Z}_n(f)}{\rho c} = \frac{\hat{S}_{AA}(f) - \hat{S}_{BB}(f) - i2\hat{Q}_{AB}(f)}{\hat{S}_{AA}(f) + \hat{S}_{BB}(f) - 2\hat{C}_{AB}(f)}$$

or

$$\frac{\hat{R}_n(f)}{\rho c} = \frac{\hat{S}_{AA}(f) - \hat{S}_{BB}(f)}{\hat{S}_{AA}(f) + \hat{S}_{BB}(f) - 2\hat{C}_{AB}(f)}, \quad (9a)$$

$$\frac{\hat{\chi}_n(f)}{\rho c} = \frac{-2\hat{Q}_{AB}(f)}{\hat{S}_{AA}(f) + \hat{S}_{BB}(f) - 2\hat{C}_{AB}(f)}, \quad (9b)$$

where $\hat{R}_n(f)$ and $\hat{\chi}_n(f)$ are the resistive and reactive impedance, respectively. Also, the power reflection coefficient $\hat{\alpha}_n(f)$ can be estimated by

$$\hat{\alpha}_n(f) = \hat{S}_{BB}(f)/\hat{S}_{AA}(f). \quad (10a)$$

Equations (9a), (9b), and (10a) are analogous to expressions for impedance and power reflection coefficient developed by assuming harmonic excitation. In the above equations the quantities $\hat{S}_{AA}(f)$ and $\hat{S}_{BB}(f)$ represent the mean-square value of the incident and reflected pressures in a narrow frequency band. The phase-shift between the incident and reflected waves is expressed in the cross-spectral density $\hat{S}_{AB}(f)$. Specifically, the phase shift $\hat{\theta}$ is

$$\hat{\theta}(f) = \tan^{-1}[\hat{Q}_{AB}(f)/\hat{C}_{AB}(f)]. \quad (10b)$$

The total pressure at two points x_1 and x_2 in the tube is

$$\tilde{p}(x_1, t) = \tilde{p}_i(x_1, t) + \tilde{p}_r(x_1, t) = [\tilde{a}(t)e^{-ik_i x_1} + \tilde{b}(t)e^{ik_r x_1}]e^{i\omega t}, \quad (11a)$$

$$\tilde{p}(x_2, t) = [\tilde{a}(t)e^{-ik_i x_2} + \tilde{b}(t)e^{ik_r x_2}]e^{i\omega t}. \quad (11b)$$

The auto- and cross-spectral densities of these two pressures are estimated by

$$\hat{S}_{11}(f) = (1/T)\{\tilde{P}_1(f, T)\tilde{P}_1^*(f, T)\}, \quad (12a)$$

$$\hat{S}_{22}(f) = (1/T)\{\tilde{P}_2(f, T)\tilde{P}_2^*(f, T)\}, \quad (12b)$$

$$\hat{S}_{12}(f) = \hat{C}_{12}(f) + i\hat{Q}_{12}(f) = (1/T)\{\tilde{P}_1(f, T)\tilde{P}_2^*(f, T)\}, \quad (12c)$$

where $\hat{S}_{11}(f)$ and $\hat{S}_{22}(f)$ are estimates of the auto-spectral densities of the pressure at points 1 and 2 and $\hat{S}_{12}(f)$ is an estimate of the cross-spectral density between the pressures at points 1 and 2; $\hat{C}_{12}(f)$ and $\hat{Q}_{12}(f)$ are the real and imaginary components of the cross-spectral density. The quantities $\tilde{P}_1(f, T)$ and $\tilde{P}_2(f, T)$ are the finite Fourier transforms of the pressure time series at points 1 and 2. By taking the Fourier transform of Eqs. (11) and combining with Eqs. (12), the following relationships are developed:

$$\hat{S}_{11}(f) = \hat{S}_{AA}(f) + \hat{S}_{BB}(f) + 2[\hat{C}_{AB}(f)\cos(k_i + k_r)x_1 + \hat{Q}_{AB}(f)\sin(k_i + k_r)x_1], \quad (13a)$$

$$\hat{S}_{22}(f) = \hat{S}_{AA}(f) + \hat{S}_{BB}(f) + 2[\hat{C}_{AB}(f)\cos(k_i + k_r)x_2 + \hat{Q}_{AB}(f)\sin(k_i + k_r)x_2], \quad (13b)$$

$$\hat{C}_{12}(f) = \hat{S}_{AA}(f)\cos k_i(x_1 - x_2) + \hat{S}_{BB}\cos k_r(x_1 - x_2) + \hat{C}_{AB}(f)[\cos(k_r x_1 + k_i x_2) + \cos(k_i x_1 + k_r x_2)] + \hat{Q}_{AB}(f)[\sin(k_r x_1 + k_i x_2) + \sin(k_i x_1 + k_r x_2)], \quad (13c)$$

$$\hat{Q}_{12}(f) = -\hat{S}_{AA}\sin k_i(x_1 - x_2) + \hat{S}_{BB}(f)\sin k_r(x_1 - x_2) + \hat{C}_{AB}(f)[-\sin(k_i x_1 + k_r x_2) + \sin(k_r x_1 + k_i x_2)] + \hat{Q}_{AB}(f)[\cos(k_i x_1 + k_r x_2) - \cos(k_r x_1 + k_i x_2)]. \quad (13d)$$

If the quantities $\hat{S}_{11}$, $\hat{S}_{22}$, $\hat{C}_{12}$, and $\hat{Q}_{12}$ are estimated from measured time records, the above equations can be solved for the unknowns $\hat{S}_{AA}(f)$, $\hat{S}_{BB}(f)$, $\hat{C}_{AB}(f)$, and $\hat{Q}_{AB}(f)$ from which the acoustic impedance and power reflection coefficient can be determined using Eqs. (9a), (9b), and (10a).

For the case with no mean flow, Eqs. (13) reduce to

$$\hat{S}_{11}(f) = \hat{S}_{AA}(f) + \hat{S}_{BB}(f) + 2[\hat{C}_{AB}(f)\cos 2kx_1 + \hat{Q}_{AB}(f)\sin 2kx_1], \quad (14a)$$

$$\hat{S}_{22}(f) = \hat{S}_{AA}(f) + \hat{S}_{BB}(f) + 2[\hat{C}_{AB}(f)\cos 2kx_2 + \hat{Q}_{AB}(f)\sin 2kx_2], \quad (14b)$$

$$\hat{C}_{12}(f) = [\hat{S}_{AA}(f) + \hat{S}_{BB}(f)]\cos k(x_1 - x_2) + 2[\hat{C}_{AB}(f) \times \cos k(x_1 + x_2) + \hat{Q}_{AB}(f)\sin k(x_1 + x_2)], \quad (14c)$$

$$\hat{Q}_{12}(f) = [-\hat{S}_{AA}(f) + \hat{S}_{BB}(f)]\sin k(x_1 - x_2). \quad (14d)$$

If a third microphone is located downstream of the system under study, the spectral density of the transmitted wave, $\hat{S}_{cc}(f)$, can be measured directly, providing an anechoic termination is used:

$$\hat{S}_{cc}(f) = (1/T)\{\tilde{P}_c(f, T)P_c^*(f, T)\}, \quad (15)$$

where $P_c(f, T)$ is the finite Fourier transform of the downstream microphone signal. The transmission loss (TL) is then given by

$$\mathrm{TL} = 10\log_{10}[\hat{S}_{AA}(f)/\hat{S}_{cc}(f)]. \quad (16)$$

II. EXPERIMENTAL METHOD

Figure 3 is a schematic showing the experimental apparatus used to evaluate the three test cases. A steel tube of nominal inside diameter of $1\frac{7}{8}$ in. (48 mm) was used for the tests, so that the plane-wave region extended to 4200 Hz. An acoustic driver was mounted at one end of the tube, and the acoustic system under study was mounted at the other end. A random noise generator provided excitation through an amplifier to the acous-

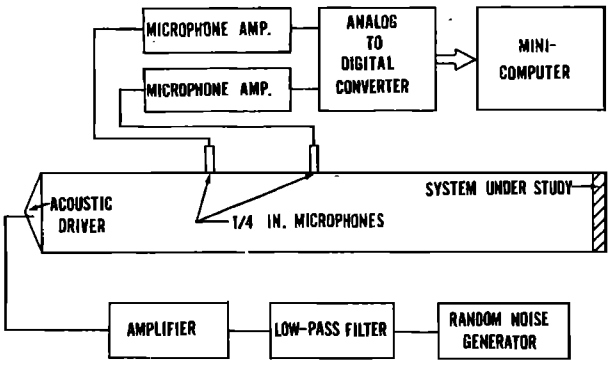

FIG. 3. Experimental set-up used in determination of impedance and power reflection coefficient using the two-microphone random-excitation method.

tic driver. A low-pass filter was used to attenuate the high-frequency portion of the input signal to prevent aliasing of the sampled data. It should be noted that the shape of the input spectrum is arbitrary providing there is sufficient energy throughout the frequency range of interest to guarantee an acceptable signal-to-noise ratio in the sound field of the tube. Flush-mounted $\frac{1}{4}$-in. microphones were used to measure the sound pressure at two points in the tube. The microphone signals were conditioned by microphone amplifiers, digitized by an analog-to-digital converter, and stored in minicomputer memory for processing. For evaluating the muffler test case (see Sec. V) an anechoic termination was attached to the downstream end of the muffler and a third microphone was flush-mounted just downstream of the muffler exit. The two upstream microphones must be sampled simultaneously for computation of the cross-spectral density $\hat{S}_{12}(f)$, but the downstream microphone can be sampled independently. Consequently, one of the upstream microphones can be used downstream and only two microphone systems are needed.

The location of the upstream microphones is not critical, within certain limitations. The microphones should be located as close to the unknown system as possible so that dissipative losses in the tube are minimized. The microphone spacing should be as small as possible for the same reason. However, each microphone is assumed to measure the sound pressure at a point in the tube, so that for very close microphone spacing the effective spacing $(x_2 - x_1)$ is difficult to estimate, particularly for large-diameter microphones. Therefore, the microphone spacing should be much larger than the diameter of the microphones used so that the effective microphone spacing can be assumed to be the distance between the microphone center lines.

III. STATISTICAL CONSIDERATIONS

Since the sound field varies randomly with time, the estimates of the microphone auto- and cross-spectra also will be random variables. It should be mentioned that the spectral estimates [Eqs. (12)] are *inconsistent* and some form of smoothing must be done to reduce the random error to an acceptable level. One method of reducing the random error of a spectrum is to divide the total time record T into n segments of equal length T_s and average individual estimates of the spectrum for each of these segments. Smoothing in this manner reduces the random error to $1/\sqrt{n}$ (e.g., for $n = 400$ the random error would be 5%), and the spectral bandwidth is $1/T_s$.

One is tempted to make T_s as small as possible so that n is very large for a given length of total time T, thereby reducing the random error to a very small value. However, this leads to a biasing of the spectrum in which spectral peaks are not resolved because the bandwidth is too wide. Consequently, the bandwidth (and therefore T_s) should be determined from a knowledge of the frequency resolution needed for the particular quantity being analyzed. This is best done experimentally by trying progressively larger bandwidths until the frequency resolution is insufficient to separate adjacent spectral peaks (note, even if the input excitation is white noise, the sound spectra may be frequency dependent because, in general, the acoustic system will be reactive).

In evaluating the three test cases a bandwidth of 20 Hz was found sufficient to resolve the sound-pressure spectra. The random error was made acceptable by averaging $n = 150$ individual spectra.

IV. CALIBRATION

In the linear range the acoustic properties are independent of the sound intensity in the tube; hence absolute calibration of the microphones is unnecessary. However, since there may be differences between the microphone and amplifier systems, a relative calibration is needed.

Since the cross-spectral density $\hat{S}_{12}(f)$ is needed for the solution of Eqs. (14), a phase calibration as well as a gain calibration is necessary.

To calibrate, the microphones were flush-mounted in a rigid circular plate attached to the end of the tube. Ideally, in this configuration both microphones would measure the same pressure amplitude with zero phase shift. Differences in microphone sensitivity and phase, as well as gain and phase differences between the microphone amplifiers, can thus be measured. The easiest method is to determine a transfer function, or frequency response, between the two microphones with the air in the tube excited by random noise. An estimate of the frequency response $H_{12}(f)$ is obtained by[7]

$$\hat{H}_{12}(f) = \hat{S}_{12}(f)/\hat{S}_{11}(f),$$

where $\hat{S}_{11}(f)$ is a smoothed estimate of the auto-spectral density of microphone 1 and $\hat{S}_{12}(f)$ is a smoothed estimate of the cross-spectral density between microphones 1 and 2. Since $\hat{S}_{12}(f)$ is a complex quantity, so is $\hat{H}_{12}(f)$ and $|\hat{H}_{12}(f)|$ is the gain between the microphones. The phase shift $\hat{\phi}_{12}(f)$ between the microphones is found by

$$\phi_{12}(f) = \tan^{-1}\frac{\mathrm{Im}[\hat{H}_{12}(f)]}{\mathrm{Re}[\hat{H}_{12}(f)]},$$

where Im and Re refer to the imaginary and real parts

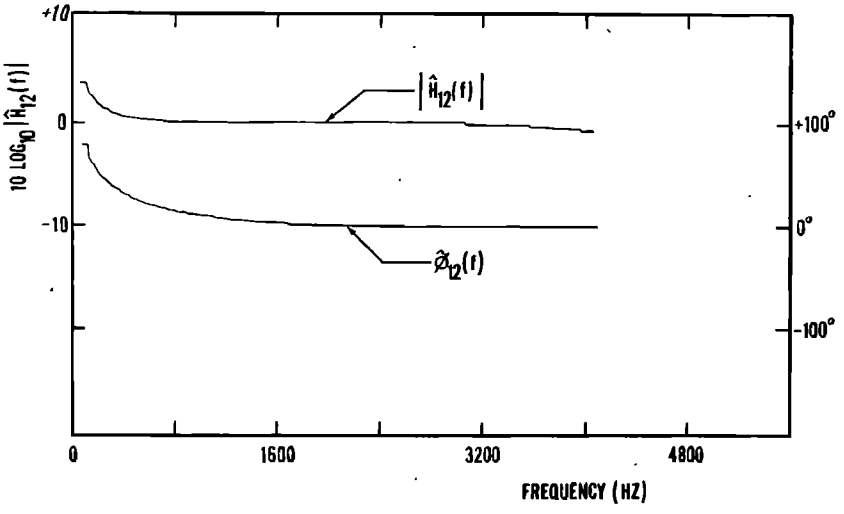

FIG. 4. Gain and phase shift between the two microphone/amplifier systems.

of $\hat{H}_{12}(f)$, respectively. Figure 4 shows the frequency response gain and phase between the two microphone/amplifier systems used in this study.

The microphone spectra for each of the test cases were corrected using the microphone frequency response calibration as follows:

$$\hat{S}_{11}(f)=[\hat{S}_{11}(f)]_u,$$

$$\hat{S}_{22}(f)=[\hat{S}_{22}(f)]_u/|\hat{H}_{12}(f)|^2,$$

$$\hat{S}_{12}(f)=[\hat{S}_{12}(f)]_u/\hat{H}_{12}(f),$$

where the subscript u refers to the uncorrected auto- and cross-spectral densities of the microphones. Note, since microphone 1 was selected (arbitrarily) as the reference microphone, $[\hat{S}_{11}(f)]_u$ does not need correcting.

V. EXPERIMENTAL RESULTS

Three test cases with zero mean flow were used to verify the two-microphone random-excitation technique. Two are classic test cases: a pipe of specified length with a rigid termination and a pipe of specified length open to free space and unbaffled. The results for each of these two cases were compared with theory, which is well developed and known to be accurate. A third and more practical test case (a prototype automotive muffler for which theory is not well developed) was also investigated and results compared to data obtained using the discrete frequency SWR method.

For the two classic test cases the following properties were determined: power reflection coefficient, phase angle between incident and reflected waves at the system input point ($x=0$), and resistive and reactive impedance. For the muffler, transmission loss and power reflection coefficient were computed, since these are the quantities of greatest importance in the design and selection of muffler elements.

The first test case (case I) evaluated was a pipe of length 4 in. (102 mm) with the same diameter as the tube holding the microphones and with a rigid circular plate covering the end, approximating zero particle velocity at $x=0$.

Assuming no losses, the resistive impedance is zero, the power reflection coefficient is unity, and the reactive impedance is given by

$$\chi_n(f)/\rho c=-\cot kL,$$

where L is the length of the tube. Figure 5 shows the experimentally determined values for the power reflection coefficient and phase angle [Eqs. (10)] for case I. Figure 6 shows the corresponding input impedance (resistive and reactive) at the open end of the tube. There is good agreement between theory and experiment at most frequencies. Since some losses are present in the

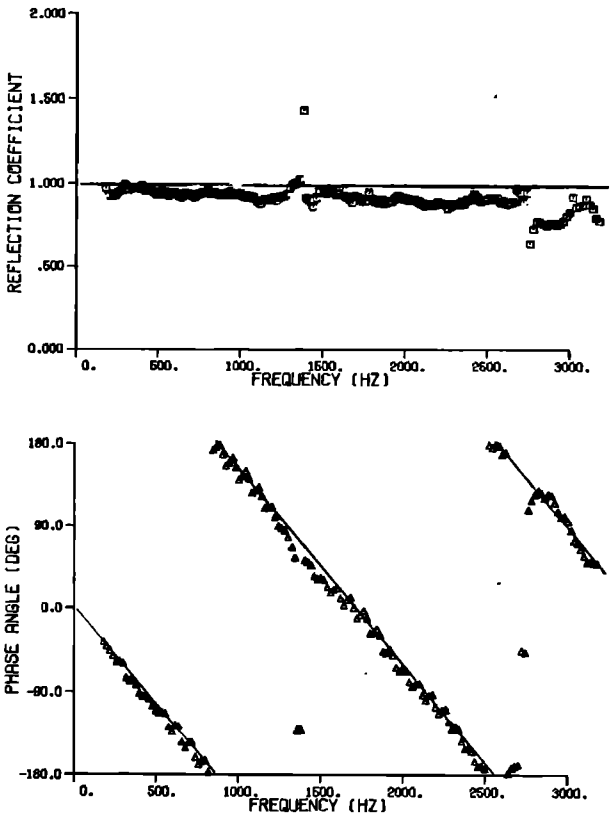

FIG. 5. Power reflection coefficient and phase angle for case I. Solid line: theory; open square, open triangle: experiment.

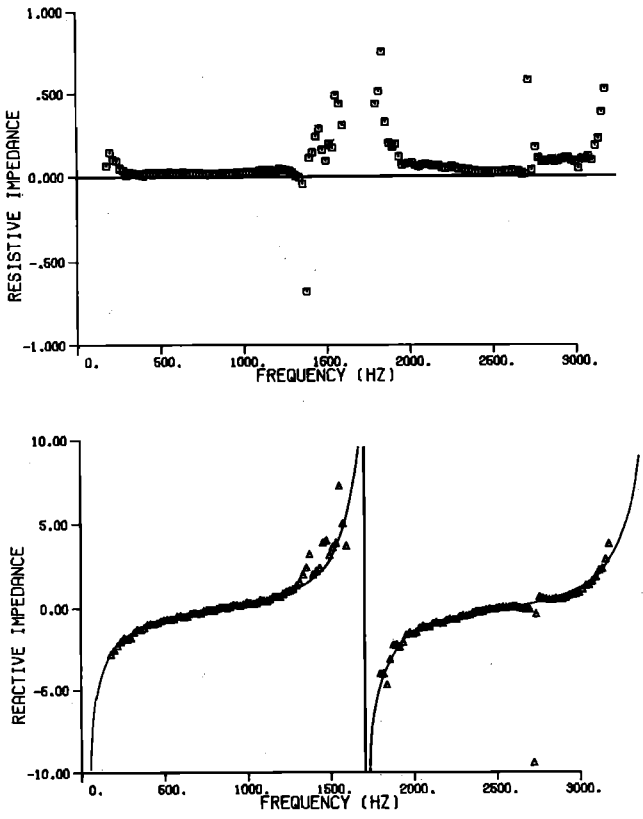

FIG. 6. Resistive and reactive impedance for case I. Solid line: theory; open square, open triangle: experiment.

tube, the reflection coefficient and resistive impedance are slightly different than the idealized values of unity and zero assumed above. The large errors in the 1500–2000-Hz range and again near 3000 Hz in both the resistive and reactive impedances are due to the indeterminate character of the impedance functions [Eqs. (9)] at frequencies where the phase angle is small ($\hat{Q}_{AB}(f) \approx 0$) for systems with high reflection coefficient [$\hat{S}_{AA}(f) \approx \hat{S}_{BB}(f)$; also $\hat{C}_{AB}(f) \approx \hat{S}_{AA}(f)$]. Under such conditions any numerical or measurement errors are magnified in the calculation of the impedance. This problem is due to the mathematical behavior of the function used for calculating impedance and is not characteristic of the two-microphone random-excitation technique. Consider the impedance function for harmonic excitation:

$$\frac{Z_n}{\rho c} = \frac{A^2 - B^2 - i2AB\sin\theta}{A^2 + B^2 - 2AB\cos\theta},$$

where A and B are the incident and reflected wave amplitudes and θ is the phase angle between the incident and reflected waves at $x = 0$. This equation is directly analogous to the impedance function developed for random excitation and will also be indeterminate when $\alpha_n \to 1$ and $\theta \to 0$. It can be shown that in the limit as $\theta \to 0$ the impedance is infinite when $\alpha_n = 1$.[8]

In Figs. 5 and 6 there are sharp discontinuities in the experimental data near 1350 and 2700 Hz which are not due to the reasons cited above. These discontinuities are due to the relationship between the microphone spacing and the wavelength at these frequencies. At 1350 Hz the microphones are spaced exactly one-half wavelength apart. At frequencies corresponding to microphone spacing of $\frac{1}{2}n\lambda$, $n = 1, 2, \ldots$, Eqs. (14) are ill conditioned. Specifically, Eq. (14a) demands that $\hat{Q}_{12}(f) = 0$ when $(x_1 - x_2) = \frac{1}{2}n\lambda$.

This problem is not a major shortcoming to the two-microphone, random-excitation method since (1) the critical frequencies at which discontinuities occur can be predicted and (2) the problem can be minimized or even circumvented. If the impedance functions, the reflection coefficient, and the transmission loss are not highly frequency dependent near the critical frequencies, the data at the critical frequencies can be ignored, and a smooth curve fitted through the remaining data. This is the case in Figs. 5 and 6 where, even with no theoretical or intuitive knowledge of the system, one can safely conclude that data at the critical frequencies result from an irregularity in the experimental method and are not due to the behavior of the system being evaluated. If one is doubtful, a second evaluation can be made with a different microphone spacing, and the new data used to supplement the initial data at the critical frequencies.

It may be possible to increase the critical frequencies above the frequency range of interest. The critical frequencies can be increased by placing the microphones very close together; but as mentioned earlier, the spacing should be much greater than the diameter of the microphones.

The experimental results for case II, an open tube of length 7.5 in. (191 mm), are shown in Figs. 7 and 8.

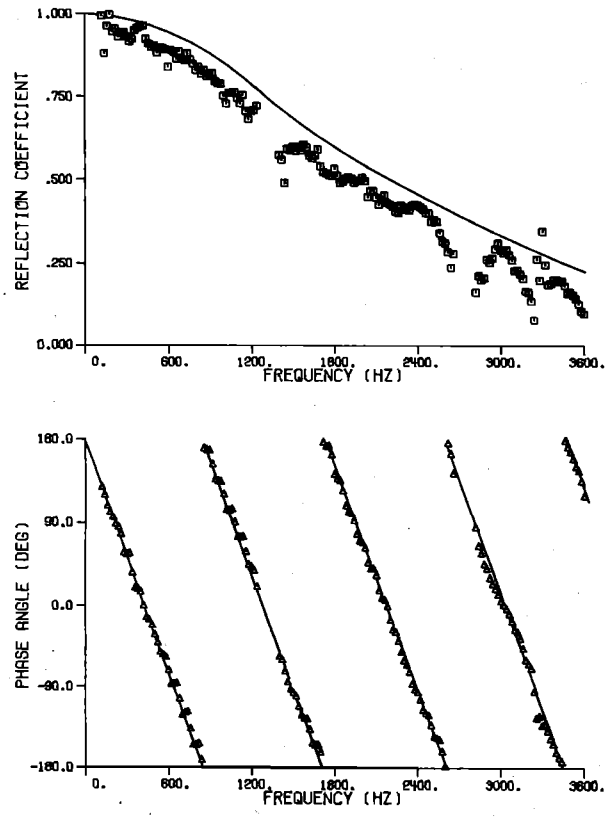

FIG. 7. Power reflection coefficient and phase angle for case II. Solid line: theory; open square, open triangle: experiment

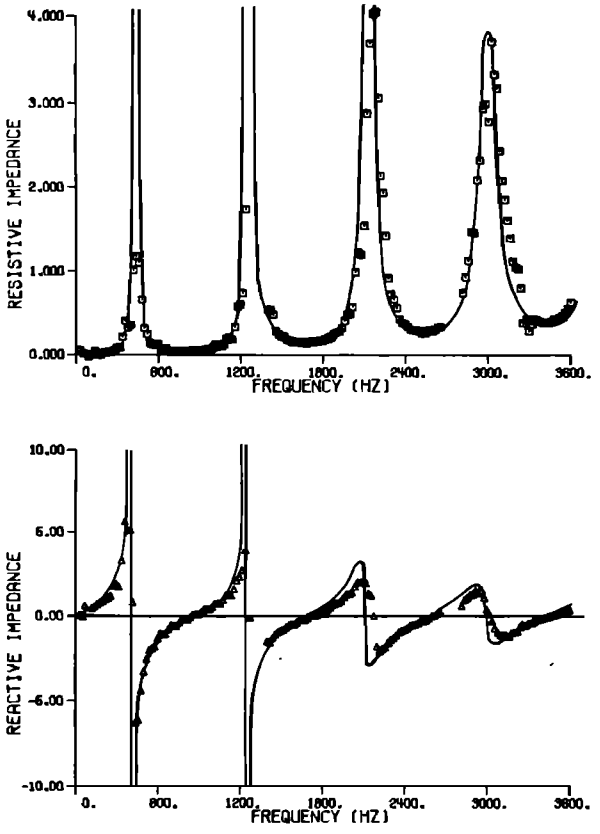

FIG. 8. Resistive and reactive impedance for case II, Solid line: theory; open square, open triangle: experiment.

The theoretical curves in these figures were obtained from Refs. 9–11. Specifically, the input impedance to the tube (assuming no losses) is given by[11]

$$\frac{Z_{in}}{\rho c}=\frac{i\sin kL+Z_r\cos kL}{iZ_r\sin kL+\cos kL},$$

where L is the length of the tube and Z_r is the radiation impedance determined by

$$Z_r=\frac{1+R}{1-R},$$

where R is the complex pressure reflection coefficient. Values of R as a function of ka are found in Ref. 9, where a is the tube radius. The power reflection coefficient is simply $|R|^2$ and the phase angle is the phase angle associated with R.[9] Agreement between theory and experiment is seen to be quite good in Figs. 7 and 8 verifying the experimental technique and, at the same time, confirming the accuracy of the theory. The discrepancies noted in Figs. 7 and 8 are similar to those witnessed by other researchers investigating radiation from open tubes.[4,12] However, as mentioned previously, the errors in the data near 1350 and 2700 Hz are due to the microphone spacing rather than a breakdown of the theory. Some of the data in these frequency ranges have been omitted to reduce the scale of the plots. The slight shifting between the theoretical and experimental data in Fig. 8 at high frequency was found to be due to having only an "approximate" value of the speed of sound. At high frequencies an error of 1% in the speed of sound shifted the data as much as 50 Hz.

The final test case examined was a prototype automotive muffler. The muffler was basically an expansion chamber with a perforated tube connecting the inlet and outlet openings. The modeling of such muffler systems is not developed well enough to make a meaningful comparison of theoretical results with experimental results obtained by the two-microphone random-excitation technique. However, the reflection coefficient was measured using the discrete frequency SWR method.

A microphone at the muffler outlet measured the downstream sound pressure which was used to compute the discrete frequency transmission loss. The muffler was also evaluated using the two-microphone random-excitation method with a downstream microphone used to measure the spectral density of the transmitted wave, $\hat{S}_{cc}(f)$, from which the transmission loss was computed, Eq. (16). Figure 9 is a comparison of the two experimental methods in estimating reflection coefficient and transmission loss for the muffler test case.

In Fig. 9 (reflection coefficient) the data in the 1200–1800 Hz range appear scattered, but upon closer examination one can see that the two methods are in very close agreement. Some of the data in the 1350- and 2700-Hz regions have been deleted from the transmission loss plot for clarity.

Apart from the data in the 1350- and 2700-Hz ranges agreement is very good considering the fact that the

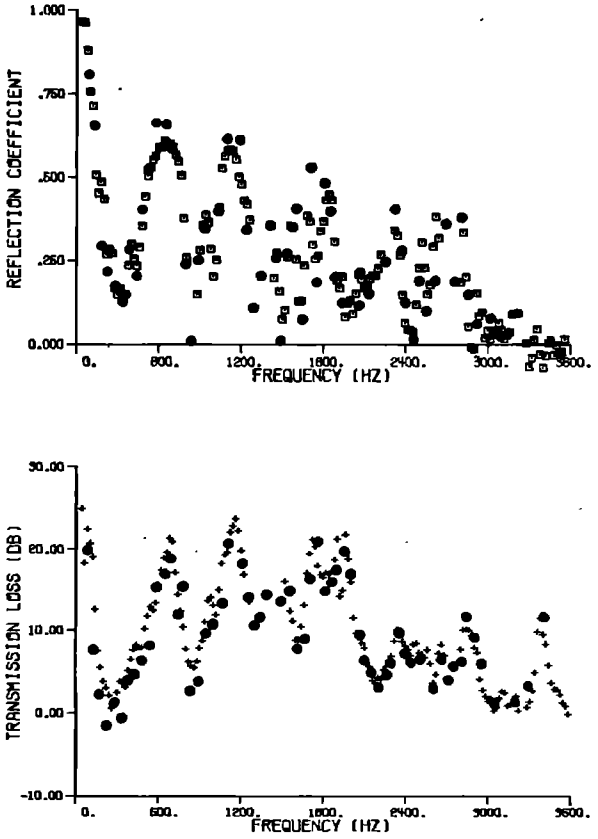

FIG. 9. Reflection coefficient and transmission loss for the prototype automotive muffler. Filled circle: SWR method; open square, plus sign: two-microphone random-excitation method.

data from the SWR method had to be corrected by probe-tube calibration data. This calibration was a least-squares fit of a curve through discrete frequency calibration data and the calibration curve had an error of approximately ±1 dB (note that the SWR transmission loss data are negative around 300 Hz).

VI. CONCLUSIONS

The two-microphone random-excitation technique has been shown to be an accurate and reliable method for the determination of normal acoustic properties.

The two-microphone random-excitation technique offers several advantages not found in other measurement techniques. The normal acoustic properties of the test cases were computed with only about 7 sec of continuous sampled data, making possible rapid evaluation of samples of porous materials or prototype acoustic filters. This is a considerable savings of time and labor as compared to the standard SWR method using microphone traversing and discrete frequency excitation. The two-microphone random-excitation technique replaces human time and labor with computer processing, an economical trade-off considering the current trends in which labor costs are increasing while computer costs are decreasing.

The use of random excitation permits the evaluation of properties at all frequencies from a single sample of data. In addition to speeding the evaluation of acoustic properties, the use of random excitation allows better frequency resolution, necessary for the evaluation of acoustic filters with acoustic properties that are highly frequency dependent. Although any bandwidth may be used, consideration must be given to the random and bias errors and the total amount of data to be sampled.

The two-microphone random-excitation technique does not require the design, construction, and calibration of a complicated probe microphone and traversing system. However, any difference in the gains or phase shift of the two microphone/amplifier systems must be known and the measured spectra corrected accordingly. This information is usually known from manufacturers' specifications, but it is recommended that a calibration test be performed such as described above.

The two-microphone random-excitation method is potentially useful for evaluating acoustic properties at low frequency, where previous methods require long tubes necessitating correction of the results for dissipation effects. This can be seen from Fig. 8, where low-frequency data were included. (Test case II was evaluated in an anechoic chamber where background noise at low frequency was minimized.)

If necessary, the microphones can be placed far enough from the system under test to minimize any near-field or higher-mode effects, a problem in measuring source impedances.

It remains to evaluate the two-microphone random-excitation technique in the presence of mean flow. Also useful would be an analysis of the statistical errors in computing the acoustic properties from the theory developed.

ACKNOWLEDGMENT

The authors would like to thank their colleague Joseph W. Sullivan for his helpful comments and for supplying the standing wave ratio data used in the study.

* This work performed while the authors were affiliated with the Ray W. Herrick Laboratories, School of Mechanical Engineering, Purdue University, West Lafayette, IN 47906.

[1] ASTM C384-58, 1972, Standard Method of Test for Impedance and Absorption of Acoustical Materials by the Tube Method.

[2] M. L. Kathuriya and M. L. Munjal, "Accurate method for the experimental evaluation of the acoustical impedance of a black box," Jr. Acoust. Soc. of Am. 58, 451–454 (1975).

[3] W. S. Gatley and R. Cohen, "Methods for Evaluating the Performance of Small Acoustic Filters," J. Acoust. Soc. Am. 46, 6–16 (1969).

[4] W. E. Schmidt and J. P. Johnston, "Measurement of Acoustic Reflection from Obstructions in a Pipe with Flow," NSF Report PD-20 (March 1975).

[5] T. H. Melling, "The Acoustic Impedance of Perforates at Medium and High Sound Pressure Levels," J. Sound Vib. 29, 1–66 (1973).

[6] R. Singh and T. Katra, "On the Dynamic Analysis and Evaluation of Compressor Mufflers," *Proceedings* 1976 *Purdue Compressor Technology Conference, July* 6–9, 1976, (Purdue University, West Lafayette, IN, 1976).

[7] J. S. Bendat and A. G. Piersol, *Random Data: Analysis and Measurement Procedures* (Wiley Interscience, New York, 1971).

[8] D. Ross, "Experimental Determination of the Normal Specific Acoustic Impedance of an Internal Combustion Engine," Ph. D. thesis (Purdue University, 1976) (unpublished).

[9] H. Levine and J. Schwinger, "On the Radiation of Sound from an Unflanged Circular Pipe," Phys. Rev. 73, 383–406 (1948).

[10] P. M. Morse and K. U. Ingard, *Theoretical Acoustics* (McGraw–Hill, New York, 1968).

[11] S. N. Rschevkin, *A Course of Lectures in the Theory of Sound* (MacMillan, New York, 1963).

[12] R. J. Alfredson, "The Design and Optimization of Exhaust Silencers," Ph. D. thesis (Institute of Sound and Vibration, Southampton, England) (unpublished).